Aggregation and Gelation in a Tunable Aqueous Colloid-Polymer Bridging System

Mariah J. Gallegos,[1] Diego D. Soetrisno,[1] Nayoung Park,[1] and Jacinta C. Conrad[1]
Department of Chemical and Biomolecular Engineering, University of Houston, Houston, TX 77204-4004

(*Electronic mail: jcconrad@uh.edu)

(Dated: 25 October 2023)

We report a colloid-polymer model system with tunable bridging interactions for microscopic studies of structure and dynamics using confocal imaging. The interactions between trifluoroethyl methacrylate-co-*tert*-butyl methacrylate (TtMA) copolymer particles and poly(acrylic acid) (PAA) polymers were controllable via polymer concentration and pH. The strength of adsorption of PAA on the particle surface, driven by pH-dependent interactions with polymer brush stabilizers on the particle surfaces, was tuned via solution pH. Particle-polymer suspensions formulated at low pH, where polymers strongly adsorbed to the particles, contained clusters or weak gels at particle volume fractions of $\phi = 0.15$ and $\phi = 0.40$. At high pH, where the PAA only weakly adsorbed to the particle surface, particles largely remained dispersed and the suspensions behaved as a dense fluid. The ability to visualize suspension structure is likely to provide insight into the role of polymer-driven bridging interactions on the behavior of colloidal suspensions.

I. INTRODUCTION

Mixtures of micron-sized colloidal particles and polymers are widely used in applications such as paints,[1,2] consumer products,[3,4] pharmaceuticals,[3] and feedstocks for 3-D printing.[5] The microscopic interactions between the particles and polymers control the mesoscale and macroscopic behavior of these suspensions. Polymers that do not adsorb onto the surface of colloidal particles induce entropic depletion attractions, whose strength and range can be tuned through the concentrations and size of the added polymer.[6–8] In applications that use flocculation or coagulation mechanisms[9–12] such as water purification[12,13] and separation processes,[14] however, polymers adsorb to the surface of the particles. In these systems, polymers can bridge between surfaces of nearby particles to generate enthalpic attractions that can alter the suspension behavior.

At low polymer concentration, chains adsorb onto the surface of one or more particles simultaneously. As the polymer concentration is increased, more chains adsorb to the surface until the surfaces of the particles are fully saturated with polymers.[6,15] In this limit, the adsorbed polymers act as steric stabilizers and particles are expected to exhibit repulsive interactions.[12] Adding polymer beyond the amount required to saturate the surfaces of the particles will not further increase the strength of bridging attractions.[16] Because the type of interaction depends on the polymer concentration, bridging systems exhibit state diagrams that are distinct from those of well-studied depletion systems. The state diagram of bridging attractions exhibits island-shaped spinodal and binodal curves,[17] in contrast to the spinodal curve that characterizes depletion-driven arrest.[18] Dynamic arrest in bridging systems is driven by kinetic arrest at the percolation line,[17] in contrast to the arrested phase separation typically observed in depletion suspensions.[19,20] The state behavior of these systems, however, depends on the microscopic interactions between the particles, which are dictated by the particle, polymer, and solution chemistries.

In one class of systems, bridging interactions driven by electrostatic attractions between oppositely-charged particles and polymers have been generated using silica particles and poly(ethylene imine)[21] and polystyrene particles and poly(*N*-isopropylacrylamide).[22,23] In a second class of systems, bridging attractions are generated by the formation of hydrogen bonds between silica particles and poly(vinyl alcohol)[24] and kaolin clay particles and polydiallyldimethylammonium chloride-C498.[25] The strength of the bridging interactions are tuned through various methods, including particle volume fraction, polymer concentration, ionic strength, and solution pH.[21,23,24] Most extant bridging systems, however, use particles that are too small to be optically resolved[24,26,27] and/or that are denser than the surrounding solvent, such that gravity may alter flocculation.[21,24]

Here, we develop a colloid-polymer bridging system in which the strength of the polymer adsorption can be tuned through the pH of the suspension and investigate its structure and dynamics. We synthesized core-shell colloidal particles composed of two different methacrylates that were sterically and electrostatically stabilized with surface-grafted polymer brushes[6,15] and refractive index- and density-matched to high dielectric solvents[7,28]. Subsequently, we induced bridging attractions between the colloidal particles by adding poly(acrylic acid) (PAA), which forms hydrogen bonds with the steric stabilizer polymer brushes on the particle surfaces. Using dynamic light scattering, we show that polymer adsorption depends on the concentration of polymer and solution pH. Using confocal microscopy, we characterize the microscopic structure and dynamics of two series of samples at constant volume fractions $\phi = 0.15$ and 0.40. As the pH is decreased, more bonds form between particles and the dynamics become increasingly arrested and more heterogeneous, consistent with aggregation. These changes in structure and dynamics are more pronounced at intermediate than at high polymer concentration in the total volume. The creation of a pH-controlled and density-matched bridging system that is compatible with confocal microscopy enables future experiments to connect particle interactions to suspension state behavior and rheolog-

ical properties.

II. MATERIALS AND METHODS

A. Particle Synthesis

All chemicals were purchased from Sigma Aldrich. Poly(2,2,2-trifluoroethyl methacrylate-co-*tert*-butyl methacrylate) (TtMA) core-shell particles were synthesized by adapting existing protocols.[7,28] Briefly, our protocol entails: (i) synthesis of fluorescent particle cores; (ii) growth of a non-fluorescent shell; and (iii) growth of charged stabilizer polymers on the particle surface. Cross-linked core-shell particles of diameter 1.63 μm with dispersity Đ = 0.07 were synthesized using a volumetric ratio of 45:55 of 2,2,2-trifluoroethyl methacrylate (TFEMA) to *tert*-butyl methacrylate (tBMA). This ratio was chosen to produce particles that could be density- and refractive index-matched to 80 (w/w)% glycerol-water. Rhodamine B methacrylate was co-reacted during core synthesis to fluorescently label particles for confocal imaging. Ethylene glycol dimethacrylate was used as a cross-linker for fluorescent monomer during core precipitation polymerization. The initiator-monomer, 2-(2-bromoisobutyryloxy)ethyl acrylate, was added during the core and shell synthesis as a sacrificial inimer to act as a growth initiator for the charged surface polymer in the final step of the synthesis. Finally, a charged copolymer of 2-acrylamido-methyl-1-propanesulfonic acid and dimethylacrylamide was grown via Atom Transfer Radical Polymerization (ATRP),[29] using a 1:1 input ratio of methanol:water to create a negatively-charged brush surface. After synthesis, the particles were collected and washed by centrifugation with de-ionized water at least five times. After final centrifugation, glycerol was added to the pellet to obtain a suspension with particle volume fraction of $\phi \sim 0.45$ in 60 (w/w)% glycerol-water. This suspension was centrifuged once more for up to 2 hours and glycerol was added to pellet to obtain a final volume fraction $\phi \sim 0.48$ in 80 (w/w)% glycerol-water. The solution was centrifuged again at 2000 g for 3 minutes to remove bubbles and then stored in a refrigerator.

B. Particle characterization

The hydrodynamic diameter of core, shell, and brush-coated TtMA particles were measured using dynamic light scattering (DLS) on an ALV-GmBH instrument (Langen, Germany) with a 5000 EPP Multiple tau Digital Correlator. Five correlation functions per angle were collected for 60 seconds for scattering angles of 60, 75, 90, 105, and 120 degrees. The temperature was held constant at 25°C using a water bath. The data were fitted using the method of cumulants using a single exponential decay,

$$g^{(2)}(\tau,q) - 1 = \beta \exp(-2\Gamma\tau)\left(1 + \frac{\mu_2}{2}\tau^2\right) \qquad (1)$$

where $\beta \approx 1$ is a correction factor that depends on the instrumental scattering geometry, $\Gamma(q)$ is the average decay rate, $\tau(q)$ is the exponential decay time, and μ_2 is the second moment of the distribution. Subsequently, we calculated the diffusion coefficient via $\Gamma = Dq^2$ and determined the hydrodynamic diameter from the Stokes-Einstein equation, $d_H = k_B T/3D\pi\eta$, where k_B is the Boltzmann constant, T is temperature, and η is the solution viscosity; we also determined the dispersity Đ= μ_2/Γ^2. We report d_H and the 95% confidence interval.

The zeta potential ζ of the particles was measured using a Nicomp 380 ZLS zeta sizer. For these measurements, the particles were diluted to $\phi = 0.001$ in a 10 mM Trizma buffer solution at pH 7.5. The zeta potential of the TtMA particles was $\zeta = -72 \pm 1$ mV, consistent with literature values.[28]

C. Polymer solution preparation

Glass vials were cleaned with toluene and left to dry. Dried vials were washed 5 times with Millipore water and placed into an oven at 100°C for 2 hours. Poly(acrylic acid) (PAA; Sigma Aldrich, 450 kDa) was weighed and poured into the clean glass vials. 5 mL of 80 (w/w)% glycerol-water was pipetted into the vial with polymer and sealed with Parafilm. Polymer stock was placed on a horizontal mixer at 7 rpm for up to 10 days until the solution was completely homogenized. Solutions were taken off the roller and stored in a desiccator.

D. Polymer adsorption characterization

To determine whether the PAA polymers adsorbed to the particle surfaces, we measured the size of particles in the presence of various low concentrations of PAA using DLS (Anton Paar instrument; Graz, Austria). We prepared suspensions of particles at $\phi = 10^{-5}$ in 80 (w/w)% glycerol-water with 5 mM NaCl and 10 mM acetate buffer at three pH values (3.8, 4.7, and 5.6) and with three concentrations of PAA (0, 0.1, and 0.2 mg mL^{-1}). Bridging suspensions were conducted at low particle fraction and polymer concentration to avoid multiple scattering during data collection. Twelve correlation functions of 60 second duration were measured for each of the nine suspensions at angles of 15, 90, and 175 degrees. The temperature was held constant at 25°C.

For suspensions without PAA, correlation functions were fit to a single-exponential cumulant function (eqn. 1). For suspensions with PAA, the DLS correlation functions were fitted using a double exponential model,

$$g^{(2)}(\tau,q) - 1 = (A_1 \exp(-\Gamma_1\tau) + A_2 \exp(-\Gamma_2\tau))^2 + \varepsilon \qquad (2)$$

where A_1 and A_2 are amplitudes and τ_1 and τ_2 are characteristic decay rates for the two species. Two diffusion coefficients $D_{\mathrm{H,X}}$ were calculated from the decay rates (eqn. 2) via $\Gamma = D_{\mathrm{H,X}}q^2$, where X = S, L. From these diffusion coefficients, we calculated hydrodynamic diameter $d_{\mathrm{H,S}}$ and $d_{\mathrm{H,L}}$ using the Stokes-Einstein equation.

E. Bridging suspension preparation

We prepared stock suspensions of colloidal particles (ϕ = 0.49) with sodium chloride (M = 70 mM) and acetate buffer (M = 50 mM), and stock solutions of PAA (12.5 and 25 mg mL^{-1}) in 80 (w/w)% glycerol-water. Stocks were tumbled horizontally in clean glass vials and then mixed to generate suspensions for imaging experiments with desired volume fraction ($\phi = 0.15$ or 0.40) and PAA concentration (0, 0.7, or 2.4 mg mL^{-1}). The concentration of PAA is given in the total sample volume and is not corrected for particle volume fraction in final suspensions. Suspensions were tumbled for 3 to 4 days for $\phi = 0.15$ and up to a week for $\phi = 0.40$ to ensure that they were homogenized. After tumbling, suspensions were centrifuged at 2000 g for 3 minutes to remove bubbles in the solution.

Glass chambers for imaging experiments were fabricated using glass cover slides and UV-curable epoxy (Norland Optical). A microscope glass slide (VWR) was cut into two 22 mm × 22 mm pieces. These glass slide pieces were attached to a glass cover slip (Gold Seal) of 48 mm × 65 mm × 0.15 mm. A third cover slip (Fisherbrand) of dimensions 22 mm × 22 mm × 0.2 was attached to the top of the cut glass slide to form a chamber. Approximately 100 μL of a given suspension was pipetted into the chamber, which was subsequently sealed using the UV-curable epoxy. The quiescent suspensions were imaged roughly 30 minutes after mixing. Confocal micrographs of bridging suspensions are shown in SI for ϕ = 0.15 (Fig. S6) and ϕ = 0.40 (Fig. S7)

F. Confocal microscopy and image analysis

A Leica DMi8 fluorescence microscope with confocal head series Leica SP8 equipped with a 63x oil-immersion objective was used to image all suspensions. To examine the 3-D structure of the suspensions, a series of 2-D images was captured at vertical positions ranging from 25 to 65 μm separated by a distance Δz of 0.1 μm. Five of these 3-D z-stacks were collected at 13.8 frames per second (fps) at different locations in the suspension. To characterize particle dynamics, 2-D images were collected as a function of time at a vertical location of 30 μm above the bottom of the coverslip. Five 2-D time series, each consisting of 1000 frames collected at 9.4 fps, were acquired at different locations in the suspension.

A particle tracking algorithm[30,31] was used to locate the particle centroids (in 2-D and 3-D) and track their position over time (in 2-D only). We report a static tracking error of ± 60 nm determined from a dilute particle suspension (ϕ = 0.05) in the absence of polymer to ensure particles are fully diffusive. The radial distribution function $g(r)$, contact number (CN), and number density fluctuation $\mathrm{NDF} = \frac{\langle \mathrm{N}^2\rangle - \langle \mathrm{N}\rangle^2}{\langle \mathrm{N}\rangle}$ were calculated from analysis of 3-D images. The ensemble-averaged mean-square displacement $\mathrm{MSD} = \langle (\mathrm{x}(\mathrm{t}+\tau) - \mathrm{x}(\mathrm{t}))^2 \rangle$ and van Hove correlation $\mathrm{G}(\mathrm{x},\mathrm{t}) = \frac{1}{\mathrm{N}} \sum_{\mathrm{n}=1}^{\infty} \delta(\mathrm{x} - [\mathrm{x_i}(\mathrm{t}) - \mathrm{x_i}(0)])$ were calculated from analysis of 2-D image time series.

III. RESULTS AND DISCUSSION

A. pH-dependent polymer adsorption drives particle aggregation

We designed an experimental system with pH-controllable bridging interactions between colloidal particles. Based on earlier studies, we expect that the interaction is driven by hydrogen bonding between PAA and either or both of the grafted polymers on the surface of the particle. The steric stabilizer, poly(vinylpyrrolidone) (PVP), forms strong hydrogen bonds with PAA at low pH;[32] likewise, the electrostablizer, N,N-dimethylacrylamide (DMA), strongly bonds to PAA under acidic conditions.[33] The strength of the hydrogen bonds is expected to decrease with increasing pH. At low pH, strong bridging interactions are expected to lead to large clusters of particles, as shown schematically in Fig. 1(a). Increasing the pH is expected to reduce the strength of polymer-mediated bridging attractions and decrease the number of polymers adsorbed on the particle surface. At sufficiently high pH, PAA is expected to have no affinity for the particle surface and no polymer adsorption is expected to occur. Thus, particles are expected to remain dispersed in solution at sufficiently high pH.

To test this picture, we assessed the extent of particle aggregation as a function of pH using dynamic light scattering (Anton Paar). The polymer concentration in this adsorption study is low enough that the effective bridging attraction between particles should increase with the polymer concentration. In the absence of polymer, the intensity-intensity correlation functions exhibit a single decay (Fig. S4(a),(d),(g)), and the hydrodynamic diameter extracted from fits of Dq^2 versus Γ is 1.65 μm. Upon addition of polymer, the intensity-intensity correlation functions exhibit two decays (Fig. S4(b),(c),(e),(f),(h),(i)). Using the Stokes-Einstein equation, we calculated two diameters $d_{\mathrm{H,S}}$ and $d_{\mathrm{H,L}}$ from the two decay times. The diameter associated with the shorter decay, $d_{\mathrm{H,S}}$, is of the order of magnitude of 20 – 90 nm and does not vary with polymer concentration or pH within the experimental error (Fig. 1(b)); thus, it likely corresponds to aggregates of free polymer in suspension. The diameter associated with the slower decay, $d_{\mathrm{H,L}}$, exceeds 1500 nm and corresponds to the typical size of a particle or aggregate of particles in solution. At pH 5.6, $d_{\mathrm{H,L}}$ grows slightly to $1.05 d_H$ as the polymer concentration is increased. At a fixed concentration of polymer, $d_{H,L}$ increases as the pH is decreased (Fig. 1(c)). Together, these results suggest that particles and polymers largely remain dispersed at pH 5.6. At lower pH, however, the sharp increase in $d_{H,L}$ upon increasing polymer concentration or decreasing pH is consistent with the formation of aggregates of increasing size. This aggregation is due to bridging of polymers between multiple particles. Thus, the DLS experiments are consistent with the schematic in Figure 1(a).

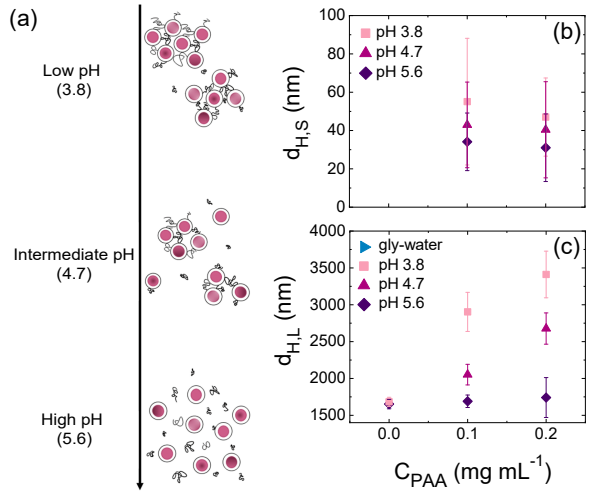

FIG. 1: (a) Schematic representation (not to scale) of hydrogen bonding between the electrostabilizer (DMA) and/or steric stabilizer (PVP) on the surface of TtMA particles (pink) and PAA (black) at pH 3.8, 4.7, and 5.6. (b) Small and (c) large hydrodynamic diameters $d_{H,S}$ and $d_{H,L}$, determined from DLS measurements (Anton Paar) on dilute particle solutions ($\phi = 10^{-5}$) as a function of polymer concentration for solutions in 80 (w/w)% glycerol-water and at pH of 3.8, 4.7, and 5.6. Error bars represent the 95% confidence interval calculated from 5 measurements.

B. Behavior at $\phi = 0.15$

To determine the effects of pH-dependent bridging on suspension behavior, we first examined the local structure of suspensions of $\phi = 0.15$ with and without added polymer and at three values of pH (3.8, 4.7, 5.6). In the absence of polymer, the radial distribution function $g(r) = 0$ for $r/2a \approx 1$ and increases to 1 for $r/2a > 1$ for all three pH values (Fig. 2(a)). The slope in $g(r)$ around $r/2a = 1$ arises from dispersity in the particles and likely a weak repulsion between the particles. This approximately step-function behavior indicates that the particles are well-dispersed and not strongly spatially correlated at any pH value investigated. We also calculated the contact number (CN) distribution, using a cutoff value of $r/2a = 1.71$ that was determined from the first minimum in $g(r)$ of the strongest gel.[34] This length scale ($r/a = 1.71$) is somewhat larger than the sum of the particle and polymer diameters. The increased size may result from any of the following: size dispersity, particle tracking error, and/or bridging distance. The contact number distribution is peaked at 2 for all suspensions (Fig. 2(b)). CN is not usually calculated in the absence of attraction due to the appearance of the peak even in concentrated suspensions of uniformly dispersed particles. We include this distribution, however, to facilitate comparison of the particle distribution in suspensions without polymer addition to the suspensions at pH 5.6, in which the particles should also be well dispersed.

Pronounced changes in $g(r)$ and the CN distributions with pH are observed upon addition of polymer. For suspensions with PAA concentration of 0.7 mg mL^{-1}, $g(r)$ approximates a step function for pH 5.6, similar to that observed in the absence of polymer (Fig. 2(c)). When the pH is lowered to 4.7, however, a sharp local maximum appears at $r/2a \approx 1$, consistent with the formation of interparticle bonds. As pH is further decreased to 3.8, the maximum at $r/2a \approx 1$ increases in height, and a second local maximum appears at $r/2a \approx 1.8$. These changes are consistent with formation of first- and second-neighbor shells often found in arrested gel-like systems.[34] We note that the value of the radius at the maximum in $g(r)$ is less than the sum of the particle size and PAA contour length (values reported in SI) but larger than the sum of the particle size and R_g. The maximum in the contact number distribution shifts to greater CN (≈ 4) as pH is decreased (Fig. 2(d)), indicating that the average number of nearest neighbors is increased. Similar structural changes with pH are observed at a higher concentration of added polymer, 2.4 mg mL^{-1}. Compared with 0.7 mg mL^{-1}, the first maximum in $g(r)$ at pH 3.8 is shorter (Fig. 2(e)). The position of the maximum in CN is 3 at low pH, indicating particles are in contact. This value is greater than that observed for suspensions without added polymer (maximum in CN at ≈ 2) but less than that in suspensions with polymer concentration 0.7 mg mL^{-1} (Fig. 2(f)).

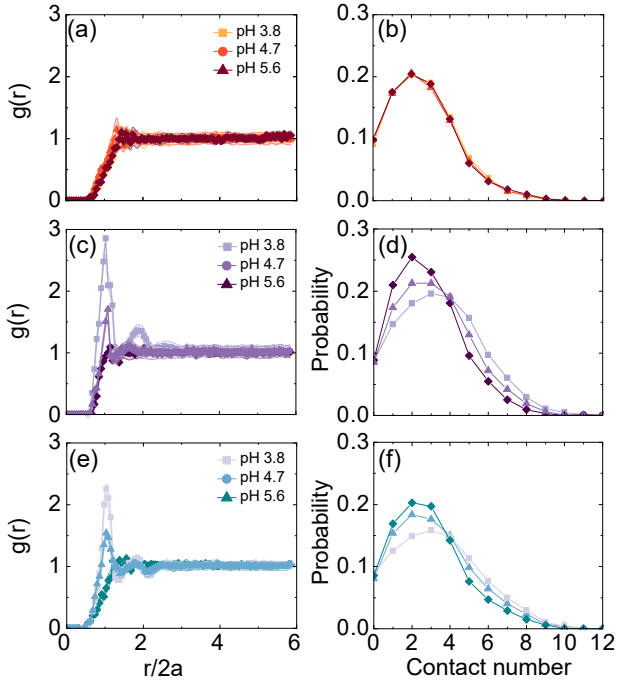

FIG. 2: (a,c,e) Radial distribution function $g(r)$ as a function of normalized distance from the particle for $\phi = 0.15$ for pH 3.8, 4.7, and 5.6 with polymer concentration of (a) 0 mg mL^{-1}, (c) 0.7 mg mL^{-1}, and (e) 2.4 mg mL^{-1}. (b,d,f) Probability distribution of contact number for $\phi = 0.15$ for pH 3.8, 4.7, and 5.6 with polymer concentration of (b) 0 mg mL^{-1}, (d) 0.7 mg mL^{-1}, and (f) 2.4 mg mL^{-1}.

The suspension structure on larger length scales also varies

with PAA concentration and pH. 3-D renderings of suspensions at constant PAA concentration of 0.7 mg mL^{-1} reveal that the structure becomes more heterogeneous as the pH is decreased from 5.6 to 3.8 (Fig. 3(a),(b),(c)). To quantify these changes in cluster structure, we calculate the number density fluctuations (NDF)[34] at a normalized length scale of $a/L = 0.16$, which corresponds to a length scale of $L = 10$ μm. This length scale was chosen as the location of the maximum in the NDF of the strongest gel (0.7 mg mL^{-1} PAA) at this ϕ; the NDF approaches one for larger values of a/L. At pH 5.6, the NDF is low and approximately independent of polymer concentration, indicating that the particles remain uniformly dispersed (Fig. 3(d)). At a fixed PAA concentration of 0.7 mg mL^{-1}, decreasing pH leads to an increase in NDF. At higher PAA concentration of 2.4 mg mL^{-1}, however, decreasing pH does not strongly affect the NDF. The high NDF value at low pH is consistent with cluster formation seen in gels, whereas the low NDF at high pH indicates that the structure is more uniform on these length scales as expected for fluids.[34,35]

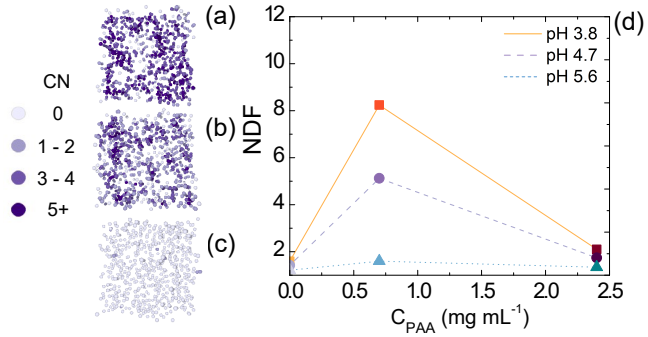

FIG. 3: (a – c) 3-D renderings (thickness $\Delta z \approx 14$ μm) of suspensions with $\phi = 0.15$ and polymer concentration of 0.7 mg mL^{-1} and pH (a) 3.8, (b) 4.7, and (c) 5.6. Particle color indicates its contact number (CN). (d) Number density fluctuation (NDF) as a function of polymer concentration C_{PAA} for suspensions with $\phi = 0.15$ and various pH, calculated at a length scale $a/L = 0.16$ that corresponds to the location of the maximum in NDF for the strongest gel.

We characterized the dynamics of particles in the suspensions by calculating the ensemble-averaged mean-square displacement (MSD) and van Hove correlation functions at a lag time $\Delta t = 5$ s. MSDs are reported in absolute time, which does not account for changes in background viscosity caused by the presence of non-bridged polymers. MSDs with rescaled delay time are presented in SI for ϕ = 0.15 and 0.4 for 0.7 mg mL^{-1} and 2.4 mg mL^{-1} to estimate the maximum slowing of dynamics due to background viscosity (Fig. S8(a-d))". For all suspensions with ϕ = 0.15 and no added polymer, the logarithmic slope of the MSD is 1, indicating that particles in these suspensions undergo normal diffusion independent of pH (Fig. 2(a)). The van Hove correlation functions for these suspensions are Gaussian, again independent of pH (Fig. 2(b)). Together, the results obtained in the absence of polymer indicate that the particles undergo Fickian diffusion, consistent with well dispersed particles at all pH values.

Upon addition of PAA, the particle dynamics depend on the pH of the solution. For ϕ = 0.15 and PAA concentration of 0.7 mg mL^{-1}, the logarithmic slope of the MSD for pH 5.6 is still approximately 1 at long lag times (Fig. 4(c)) and the van Hove distributions are Gaussian (Fig. 4(d)), as also observed for suspensions without PAA. Upon decreasing the pH to 4.7, however, the MSD is smaller than that at pH 5.6 on long time scales and the logarithmic slope is less than 1. The van Hove correlation function for this suspension exhibits extended tails at high displacements. When the pH is further decreased to 3.8, the MSD is more subdiffusive (lower logarithmic slope at long times) and the van Hove correlation function is more non-Gaussian when compared to the suspensions at pH 4.7. The decrease in MSD and the development of non-Gaussian tails in the van Hove correlation functions[35,36] are consistent with increasing aggregation of the particles as pH is decreased below 5.6.

When the PAA concentration is further increased to 2.4 mg mL^{-1}, the dynamics do not exhibit strong changes with pH. The MSDs for these suspensions are subdiffusive for all pH values and have similar logarithmic slopes on long time scales (Fig. 4(e)) and the van Hove correlation functions are slightly non-Gaussian at all pH values (Fig. 4(f)). These results suggest that increasing the concentration of PAA to 2.4 mg mL^{-1} leads to dynamics that are consistent with aggregation, but the extent of aggregation appears to be less than that observed at PAA concentration of 0.7 mg mL^{-1}.

Together, the measurements of structure and dynamics for suspensions with $\phi = 0.15$ and various concentration of PAA indicate that suspension behavior can be tuned through both polymer concentration and pH. In the absence of PAA, particles are well dispersed, as indicated by fluid-like structure and Fickian diffusion. Upon addition of 0.7 mg mL^{-1} PAA, pronounced changes in particle structure and dynamics at low pH are consistent with aggregation. When the concentration of PAA is further increased to 2.4 mg mL^{-1}, changes in structure and dynamics consistent with aggregation are still observed but are less pronounced than those observed at lower PAA concentration.

One explanation for the weaker aggregation at higher polymer concentration is that the surfaces of the particles may become saturated with the bridging polymer.[37] Such saturation is sometimes observed in bridging systems. For example, in a system of polystyrene microspheres and poly(N-isopropylacrylamide) microgels,[22] high concentrations of the microgel bridging agent led to complete surface saturation of the microspheres and to depletion attractions that were weaker than the low-microgel-concentration bridging attractions.[22] Thus, we conducted steric stabilization experiments (Fig. S10 in the SI) and determined that steric stabilization for $\phi = 0.15$ occurs at 5.7 $\pm$ 0.6 mg mL^{-1}. Thus, at 2.4 mg mL^{-1}, it is likely that some of the particles have become saturated with polymer, consistent with the weaker structure formation. Thus, the attractive bridging interactions that dictate the suspension properties may be partially mitigated by steric repulsion when the concentration of added polymer is sufficiently high.

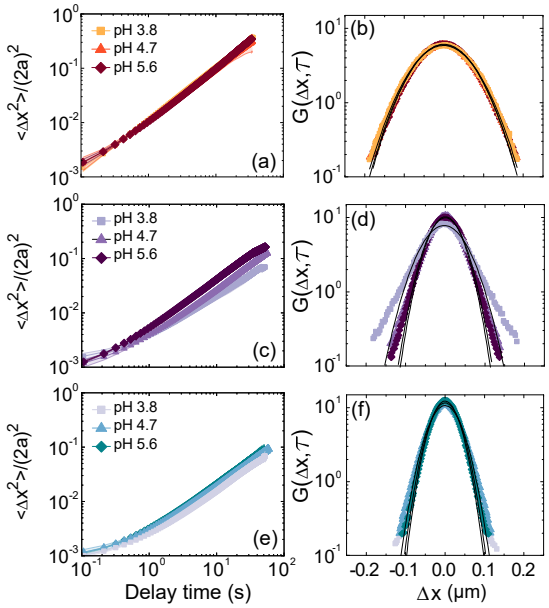

FIG. 4: (a, c, e) Normalized MSD$\langle \Delta x^2 \rangle / (2a)^2$ as a function of delay time τ for $\phi = 0.15$ suspensions with (a) 0 mg mL^{-1}, (c) 0.7 mg mL^{-1}, and (e) 2.4 mg mL^{-1} PAA and pH 3.8 (squares), 4.7 (triangles), and 5.6 (diamonds). (b,d,f) van Hove correlation functions as a function of displacement Δx (μm) at τ = 5 seconds for $\phi = 0.15$ suspensions with (b) 0 mg mL^{-1}, (d) 0.7 mg mL^{-1}, and (f) 2.4 mg mL^{-1} PAA and pH 3.8 (squares), 4.7 (triangles), and 5.6 (diamonds).

C. Behavior at $\phi = 0.40$

We also investigated the behavior of the tunable bridging system at a higher particle volume fraction of $\phi = 0.40$, where the average distance between particles (≈ 1.4 μm) is smaller than that at $\phi = 0.15$ (≈ 4.7 μm). In the absence of polymer, the pair correlation functions $g(r)$ measured at pH 3.8, 4.7, and 5.6 exhibit two local maxima: the maximum at $r/2a \approx 1$ corresponds to the interparticle separation, whereas the maximum at $r/2a \approx 2$ corresponds to the formation of a second-neighbor shell expected for dense systems (Fig. 5(a)). The local maximum in contact number shifts to higher CN ≈ 4 as compared to the $\phi = 0.15$ suspensions, consistent with the greater particle density (Fig. 5(b)).

Addition of polymer at a concentration of 0.7 mg mL^{-1} does not qualitatively alter $g(r)$ or the CN distribution at pH 5.6, indicating that the structure remains that of a dense suspension (Fig. 5(c)). Upon decreasing the pH to 4.7, however, the local maximum at $r/2a \approx 1$ increases in height, consistent with the formation of interparticle bonds. The position of the maximum in CN shifts to the right, indicating that the average number of nearest neighbors increases (Fig. 5(d)). A further decrease in the the pH, to 3.8, leads to an additional increase in the height of the local maximum, consistent with enhanced structural correlations. At pH 3.8, however, the average number of nearest neighbors is similar to that at pH 4.7.

At the highest polymer concentration investigated, 2.4 mg mL^{-1}, decreasing pH also leads to structural changes that are consistent with increased bond formation. The magnitude of the changes in local structure with pH, however, are less pronounced than those observed at 0.7 mg mL^{-1}. For example, both the maximum in $g(r)$ at $r/2a \approx 1$ and the local maximum at $r/2a \approx 2$ are shorter at high pH (Fig. 5(e)). Likewise, the series at 2.4 mg mL^{-1} exhibits a modest shift in the CN distribution to the right with increasing pH (Fig. 5(f)). The weaker structural evolution at higher polymer concentration is consistent with the trend observed for $\phi = 0.15$. Similar behavior was observed in a silica-poly(ethylene imine) bridging system at $\phi = 0.3$, where the contact number did not appreciably increase at high polymer concentration.[21] In Ref. 21, the lack of structural changes at high polymer concentration was attributed to the high level of crowding in these suspensions. In our $\phi = 0.40$ systems, we posit that lack of structural evolution with increasing polymer concentration is also due to the high crowding.

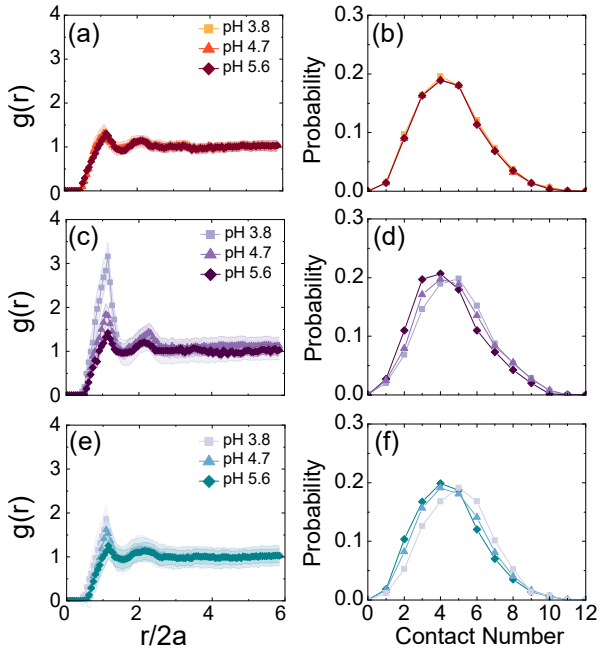

FIG. 5: (a,c,e) Radial distribution function $g(r)$ as a function of normalized distance from the particle for $\phi = 0.40$ for pH 3.8, 4.7, and 5.6 with polymer concentration of (a) 0 mg mL^{-1}, (c) 0.7 mg mL^{-1}, and (e) 2.4 mg mL^{-1}. (b,d,f) Probability distribution of contact number for $\phi = 0.40$ for pH 3.8, 4.7, and 5.6 with polymer concentration of (b) 0 mg mL^{-1}, (d) 0.7 mg mL^{-1}, and (f) 2.4 mg mL^{-1}.

Changes in local structure with pH are again accompanied by structural changes on large length scales for $\phi = 0.40$ suspensions. Reconstructions of confocal micrographs for a series of suspensions with 0.7 mg mL^{-1} show that the structure becomes increasingly heterogeneous as the pH is decreased (Fig. 6(a),(b),(c)). Following the protocol used for $\phi = 0.15$ in Figure 3(d), we calculate the NDF at $a/L = 0.10$, corresponding to a length scale of 16 μm, for which the strongest gel for $\phi = 0.40$ exhibits a maximum in the NDF. For all $\phi = 0.40$

suspensions, the NDF at a given pH and polymer concentration is less than that of the corresponding suspensions with $\phi = 0.15$ (Fig. 6(d)), reflecting the greater structural uniformity expected at higher ϕ. Trends in NDF upon changing system parameters are qualitatively similar to those observed at $\phi = 0.15$: the NDF is independent of pH in the absence of polymer and independent of polymer concentration at pH 5.6; as the pH is decreased from 5.6 to 3.8, the NDF increases markedly for polymer concentration 0.7 mg mL^{-1} but only slightly for polymer concentration 2.4 mg mL^{-1}. As also observed for $\phi = 0.15$ suspensions, the NDF for $\phi = 0.40$ suspensions with polymer concentration of 2.4 mg mL^{-1} is less than that at 0.7 mg mL^{-1} for equal pH. The decrease in NDF between $\phi = 0.15$ and 0.4 suspensions is due to the decrease in compressibility and increased uniformity at higher particle volume fraction.[34,38]

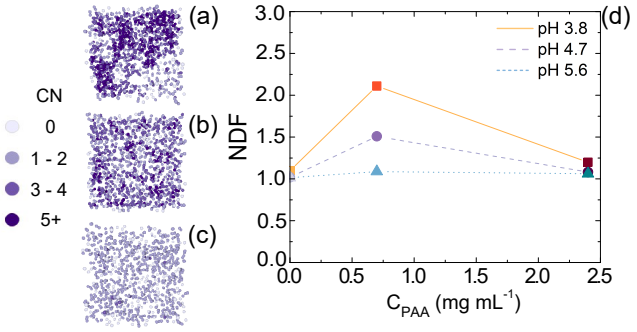

FIG. 6: (a – c) 3-D renderings (thickness $\Delta z \approx 14\ \mu$m) of suspensions with $\phi = 0.40$ and polymer concentration of 0.7 mg mL^{-1} and pH (a) 3.8, (b) 4.7, and (c) 5.6. Particle color indicates its contact number (CN). (d) Number density fluctuation (NDF) as a function of polymer concentration C_{PAA} for suspensions with $\phi = 0.40$ and various pH, calculated at a length scale $a/L = 0.10$ that corresponds to the location of the maximum in NDF for the strongest gel.

Finally, we examined the dynamics of suspensions with $\phi = 0.40$. The MSD of a $\phi = 0.40$ suspension with a given pH and polymer concentration is lower than that of the corresponding suspension at $\phi = 0.15$, reflecting the slowing of dynamics at higher particle concentration. In the absence of polymer, the MSD scales as a power law with exponent < 1 at long delay times, indicating that the suspension dynamics are subdiffusive as expected for dense fluids (Fig. 7(a)). The van Hove correlation functions exhibit slight non-Gaussian tails, consistent with dynamic heterogeneity, but do not change as a function of pH (Fig. 7(b)). For suspensions with polymer concentration of 0.7 mg mL^{-1}, decreasing the pH leads to dynamics that are slower and increasingly subdiffusive; at pH 3.8, the MSD is nearly constant for $\Delta t < 10$ s, indicating that particles are nearly arrested on these time scales ((Fig. 7(c)). The van Hove correlation functions exhibit non-Gaussian tails, again consistent with dynamical heterogeneity (Fig. 7(d)). At the highest polymer concentration, 2.4 mg mL^{-1}, the MSD again decreases in magnitude and becomes more subdiffusive as pH is decreased, but the extent of changes are less pronounced than for the lower polymer concentration ((Fig. 7(e)); the corresponding van Hove correlation functions became slightly more non-Gaussian ((Fig. 7(f)). Together, the dynamic metrics for $\phi = 0.40$ samples are consistent with a decrease in available free volume space occupied by particles and polymers. Curvature in $\phi = 0.40$ (Figs. 7(a,c,e)) reflects crossover between dynamic regimes arising from the presence of disperse aggregates.

The measurements of structure and dynamics for suspensions with $\phi = 0.40$ and various concentrations of PAA show that tuning the bridging interaction through pH can be used to modulate arrest in dense suspensions. Whereas a dense fluid without appreciable clustering is observed in the absence of added polymer, changes in suspension structure and dynamics upon lowering pH in suspensions with 0.7 mg mL^{-1} are consistent with the formation of a space-spanning arrested network. Qualitatively similar but quantitatively smaller changes with pH are observed for suspensions with 2.4 mg mL^{-1}. The polymer concentrations are far below that needed for steric stabilization at $\phi = 0.40$, 15 ± 2 mg mL^{-1}, suggesting that the modest changes with pH observed at higher polymer concentration are a result of crowding by particles and polymers.

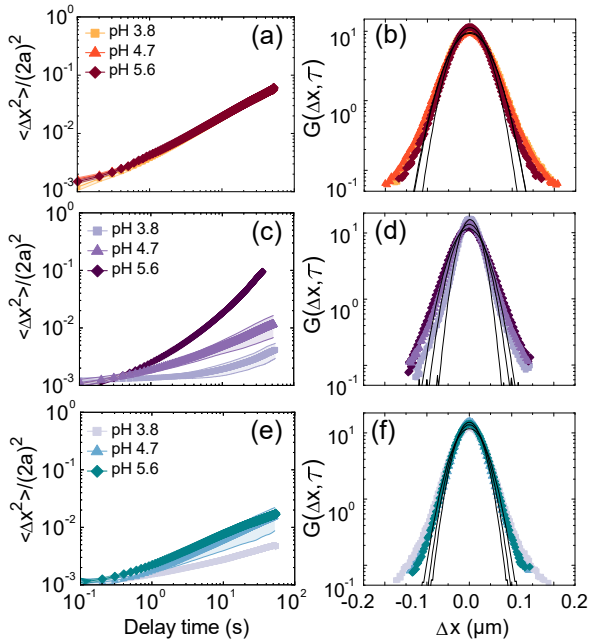

FIG. 7: (a, c, e) Normalized MSD$\langle \Delta x^2 \rangle / (2a)^2$ as a function of delay time τ for $\phi = 0.40$ suspensions with (a) 0 mg mL^{-1}, (c) 0.7 mg mL^{-1}, and (e) 2.4 mg mL^{-1} PAA and pH 3.8 (squares), 4.7 (triangles), and 5.6 (diamonds). (b,d,f) van Hove correlation functions as a function of displacement Δx (μm) at $\tau = 5$ seconds for $\phi = 0.40$ suspensions with (b) 0 mg mL^{-1}, (d) 0.7 mg mL^{-1}, and (f) 2.4 mg mL^{-1} PAA and pH 3.8 (squares), 4.7 (triangles), and 5.6 (diamonds).

IV. CONCLUSION

We developed a model bridging system consisting of TtMA copolymer particles and an adsorbing polymer, PAA, where the interparticle interactions can be tuned through the pH, polymer concentration, and particle concentration, and showed how changes in the interactions affect suspension structure and dynamics using confocal microscopy. With the addition of polymer (0.7 mg mL^{-1}), suspension properties could be tuned from fluid-like at high pH to clustered or gel-like at low pH. A transition to solid-like behavior upon decreasing the pH was also observed at a polymer concentration of 2.4 mg mL^{-1}, but the structural and dynamic changes with pH were less pronounced than those observed at lower polymer concentration. For $\phi = 0.15$, this finding likely reflects the onset of steric stabilization of some of the particles, whereas at $\phi = 0.40$ this finding likely reflects the overall high crowding in these suspensions.

We have shown that variation of interparticle interactions in a bridging system through pH and polymer concentration can lead to stronger or weaker gels. The interparticle interactions in the bridging system reported here can be tuned through pH and polymer concentration. Further, this system is compatible with confocal imaging and is suitable for rheological measurements. Thus, we anticipate that this system will enable studies of microstructure-property relationships in flocculated colloidal suspension. For example, the chemistry of this system is similar to our earlier-developed depletion system[7], and thus can be used to directly compare the structures formed under entropic (depletion) versus enthalpic (bridging) interactions. In addition, polymers adsorbed to the particle surface can also generate interesting rheological properties such as shake-gels[26], rheopexy,[39,40] and thixotropy.[40,41] We anticipate that this system can be used to investigate the microstructural origins of these interesting flow properties by tuning the particle and polymer sizes.

FUNDING

This work was supported by the National Science Foundation (CBET-1803728) and the Welch Foundation (E-1869).

ACKNOWLEDGEMENTS

We thank Peter Vekilov for use of his dynamic light scattering setup (ALV-GmBH instrument; Langen, Germany) and Alamgir Karim for the use of his dynamic light scattering setup (Litesizer instrument; Graz, Austria).

DATA AVAILABILITY STATEMENT

The data that support the findings of this study are available from the corresponding author upon reasonable request.

[1] R. Lambourne and T. A. Strivens, "Paint and surface coatings: Theory and practice," (1999).
[2] F. Karakas and M. S. Celik, "Stabilization mechanism of main paint pigments," Prog. Org. Coat. **123**, 292–298 (2018).
[3] C. Gallegos and J. M. Franco, "Rheology of food, cosmetics and pharmaceuticals," Curr. Opin. **4**, 288–293 (1999).
[4] C. Wibowo and K. M. Ng, "Product-centered processing: Manufacture ofchemical-based consumer products," AIChE Journal **48**, 1212–1230 (2002).
[5] M. Areir, Y. Xu, D. Harrison, and J. Fyson, "3d printing of highlyflexible supercapacitor designed for wearable energystorage," Mater. Sci. Eng. B **226**, 29–38 (2017).
[6] P. C. Hiemenz and R. Rajagopalan, "Principles of colloid and surface chemistry," .
[7] N. Park, E. J. Umanzor, and J. C. Conrad, "Aqueous colloid + polymer depletion system for confocal microscopy and rheology," Front. Phys. **6**, 42 (2018).
[8] L. Sapir and D. Harries, "Macromolecular compaction by mixed solutions: Bridging versus depletion attraction," Curr. Opin. Colloid Interface Sci. **22**, 80–87 (2016).
[9] R. I. Jeldres, F. Concha, and P. G. Toledo, "Population balance modelling of particle flocculation with attention to aggregate restructuring and permeability," Adv. Colloid Interface Sci. **224**, 62–71 (2015).
[10] E. Dickinson and L. Eriksson, "Particle flocculation by adsorbing polymers," Adv. Colloid Interface Sci. **34**, 1–29 (1991).
[11] G. Liang, A. V. Nguyen, W. Chen, T. A. H. Nguyen, and S. Biggs, "Interaction forces between goethite and polymeric flocculants and their effect on the flocculation of fine goethite particles," Chem. Eng. Sci. **334**, 1034–1045 (2018).
[12] Y. D. Yan, S. M. Glover, G. J. Jameson, and S. Biggs, "The flocculation efficiency of polydisperse polymer flocculants," Int. J. Miner. **73**, 161–175 (2004).
[13] B. Bolto and J. Gregory, "Organic polyelectrolytes in water treatment," Water Res. **41**, 2301–2324 (2007).
[14] E. J. H. Wee, T. H. Ngo, and M. Trau, "A simple bridging flocculation assay for rapid, sensitive and stringent detection of gene specific dna methylation," Sci. Rep. **5**, 15028 (2015).
[15] S. Biggs, "Steric and bridging forces between surfaces bearing adsorbed polymer: An atomic force microscopy study," Langmuir **11**, 156–162 (1995).
[16] J. Chen, S. R. Kline, and Y. Liu, "From the depletion attraction to the bridging attraction: the effect of solvent molecules on the effective colloidal interactions," J. Chem. Phys. **142**, 084904 (2015).
[17] G. Yuan, J. Luo, C. C. Han, and Y. Liu, "Gelation transitions of colloidal systems with bridging attractions," Phys. Rev. E **94**, 040601 (2016).
[18] S. M. Ilett, A. Orrock, W. C. K. Poon, and P. N. Pusey, "Phase behavior of a model colloid-polymer mixture," Phys. Rev. E **51**, 1344–1352 (1995).
[19] S. Manley, L. Cipelletti, V. Trappe, A. E. Bailey, R. J. Christianson, U. Gasser, V. Prasad, P. N. Segre, M. P. Doherty, S. Sankaran, A. L. Jankovsky, B. Shiley, J. Bowen, J. Eggers, T. Kurta, C. amd Lorik, and D. A. Weitz, "Limits to gelation in colloidal aggregation," PRL **93**, 108302 (2004).
[20] C. M. Fellows and W. O. S. Doherty, "Insights into bridging flocculation," Macromol. Symp. **231**, 1–10 (2006).
[21] K. Pickrahn, B. Rajaram, and A. Mohraz, "Relationship between microstructure, dynamics, and rheology in polymer-bridging colloidal gels," Langmuir **26**, 2392–2400 (2010).
[22] C. Zhao, G. Yuan, D. Jia, and C. C. Han, "Macrogel induced by microgel: bridging and depletion mechanisms," Soft Matter **8**, 7036 (2012).
[23] C. Zhao, G. Yuan, and C. C. Han, "Bridging and caging in mixed suspensions of microsphere and absorptive microgel," Soft Matter **10**, 8905–8912 (2014).
[24] S. Kim, J. H. Sung, K. H. Ahn, and S. J. Lee, "Adsorption–stress relationship in drying of silica/pva suspensions," J. Colloid Interface Sci. **361**, 497–502 (2011).
[25] J. Yu, D. Wang, G. Xiaopeng, M. Yan, and M. Y. Yang, "Flocculation of kaolin particles by two typical polyelectrolytes: A comparative study on the kinetics and floc structures," Colloid Surf. A–Physicochem. Eng. Asp. **290**, 288–294 (2006).
[26] J. Zebrowski, V. Prasad, W. Zhang, L. M. Walker, and D. A. Weitz, "Shake-gels: shear-induced gelation of laponite–peo mixtures," Colloid Surf. A–

Physicochem. Eng. Asp. **213**, 129–197 (2003).
[27] S. Kawasaki and M. Kobayashi, "Affirmation of the effect of ph on shake-gel and shear thickening of a mixed suspension of polyethylene oxide and silica nanoparticles, colloids and surfaces a: Physicochemical and engineering aspects," Colloid Surf. A–Physicochem. Eng. Asp. **537**, 236–242 (2018).
[28] T. E. Kodger, R. E. Guerra, and J. Sprakel, "Precise colloids with tunable interactions for confocal microscopy," Sci. Rep. **5**, 1436 (2015).
[29] C. Perruchot, M. A. Khan, A. Kamitsi, S. P. Armes, T. von Werne, and T. E. Patten, "Synthesis of well-defined, polymer-grafted silica particles by aqueous atrp," Langmuir **17**, 4479–4481 (2001).
[30] J. C. Crocker and D. G. Grier, "Methods of digital video microscopy for colloidal studies," J. Colloid Interface Sci. **179**, 298–310 (1996).
[31] D. Blair and E. Dufresne, "The matlab particle tracking code repository," .
[32] Pradip, C. Maltesh, P. Somasundaran, R. A. Kulkarni, and S. Gundiah, "Polymer-polymer complexation in dilute aqueous solutions: poly(acrylic acid)-poly(ethylene oxide) and poly(acrylic acid)-poly(vinylpyrrolidone)," Langmuir **7**, 2108–2111 (1991).
[33] Y. Wang and H. Morawetz, "Fluorescence study of the complexation of poly(acrylic acid) with poly(n,n-dimethylacrylamide-co-acrylamide)," Macromolecules **22**, 164–167 (1989).
[34] C. L. Dibble, M. Kogan, and M. J. Solomon, "Structure and dynamics of colloidal depletion gels: Coincidence of transitions and heterogeneity," Phys. Rev. Lett. E. **74**, 041403 (2006).
[35] Y. Gao and M. L. Kilfoil, "Direct imaging of dynamical heterogeneities near the colloid-gel transition," Phys. Rev. Lett. **99**, 078301 (2007).
[36] B. Wang, J. Kuo, S. C. Bae, and S. Granick, "When brownian diffusion is not gaussian," Nat. Mater. **11**, 481–485 (2012).
[37] A. G. Garcia, M. M. Nagelkerke, R. Tuinier, and M. Vis, "Polymer-mediated colloidal stability: on the transition between adsorption and depletion," Adv. Colloid Interface **275**, 102077 (2020).
[38] M. Kogan, C. J. Dibble, R. E. Rogers, and M. J. Solomon, "Viscous solvent colloidal system for direct visualization of suspension structure, dynamics and rheology," J. Colloid Interface Sci. **318**, 252–263 (2008).
[39] G. Ovarlez, L. Tocquer, F. Bertranda, and P. Coussota, "Rheopexy and tunable yield stress of carbon black suspensions," Soft Matter **9**, 5540–5549 (2013).
[40] A. Potanin, "Thixotropy and rheopexy of aggregated dispersions with wetting polymer," J. Rheol. **48**, 1279 (2004).
[41] N. Koumakis, E. Moghimi, R. Besseling, W. C. K. Poon, J. F. Brady, and G. Petekidis, "Tuning colloidal gels by shear," Soft Matter **11**, 4640 (2015).